The magneto-structural relationship in the tetrahedral spin chain oxide $CsCoO_2$

N. Z. Ali,[1] R. C. Williams,[2] F. Xiao,[2] S. J. Clark,[2] T. Lancaster,[2] S. J. Blundell,[3] D. V. Sheptyakov,[4] and M. Jansen[1]

[1] *Max-Planck-Institut für Festkörperforschung, Heisenbergstr. 1, D-70569 Stuttgart, Germany*
[2] *Durham University, Department of Physics, South Road, Durham, DH1 3LE, UK*
[3] *Oxford University Department of Physics, Parks Road, Oxford, OX1 3PU, UK*
[4] *Laboratory for Neutron Scattering, Paul Scherrer Institut, CH-5232 Villigen, Switzerland*

(Dated: September 26, 2014)

We have investigated the structural and magnetic transitions in $CsCoO_2$ using calorimetric measurements, neutron powder diffraction (NPD), density functional theory (DFT) calculations and muon-spin relaxation (μSR) measurements. $CsCoO_2$ exhibits three-dimensional long-range antiferromagnetic (AFM) order at 424 K, resulting in antiferromagnetic alignment of chains of ferromagnetically ordered Co-Co spin dimers. Although there is no change in magnetic structure around a structural transition at $T^* = 100$ K, the resulting bifurcation of corner sharing Co–O–Co bond angles causes a weakening of the AFM interaction for one set of bonds along the chains. Consequently, the system undergoing a complex freezing out of relaxation processes on cooling.

PACS numbers: XXXX.XXXX

Cobalt-based multinary oxides continue to attract significant interest due to their complex phase diagrams and the richness of their magnetic and electronic properties, induced by strong correlation between spin, charge, and orbital degrees of freedom. Together with chemical composition and synthesis conditions, the spin states in oxocobaltates are sensitive to external physical parameters such as temperature and pressure. A subtle energy balance between the crystal field splitting and Hunds rule exchange energy in the $3d$ states ultimately regulates the spin state of individual Co ions, offering new potential for tuning materials properties.[1–3] The most commonly encountered coordination geometry in multinary oxocobaltates(III), ($3d^6$), is octahedral, resulting in the low-spin electron configuration ($S = 0$; $t_{2g}^6 e_g^0$). The less commonly observed tetrahedral coordination geometry, with the weaker crystal field splitting, favours the high-spin state ($S = 2$; $e_g^3 t_{2g}^3$).[4–8] Within the AMO_2 family of ternary oxides, the recently discovered $CsCoO_2$ features a singular crystal structure.[9] Here Co^{3+} is again in a tetrahedral coordination with edge-linked CoO_4 tetrahedra forming 'bow-tie' shaped $Co_2O_6^{6-}$ dimers which are then connected via corner-shared oxygen ions to form spin chains, creating an overall butterfly motif.

The special connectivity engendered by this architecture leads to very strongly coupled antiferromagnetism. According to the Goodenough-Kanamori-Anderson (GKA) rules the interdimer superexchange interaction (mediated via corner-shared oxygen ions, denoted O2) the Co–O2–Co bonding angle between neighboring Co atoms lies close to 180°; hence the subsequent interaction between partially filled d orbitals is strongly anitferromagnetic (AFM). Conversely, intradimer Co–Co neighbors are coupled through the intervening edge-shared oxygen ions (denoted O1) with bonding angles close to 90°, and hence the superexchange interaction is expected to be ferromagnetic (FM). Measurements of the magnetic susceptibility[9] show that the consequence of the connectivity between Co^{3+} ions in such a structure is canted antiferromagnetic order below the remarkably high temperature of $T_N = 430$ K. Above the ordering temperature the susceptibility becomes temperature independent, suggesting the persistence of very strong exchange coupling. Despite the progress made in understanding this system, the magnetic behaviour that accompanies a structural transition that occurs around 100 K (hereafter denoted T^*), involving a monoclinic distortion resulting from a tilting of the edge-sharing tetrahedra, remains poorly understood. We have therefore carried out a detailed investigation into the magnetism of this system, whose aim is to determine the low energy model of spin interactions and to elucidate both the nature of the ordering transition and the magnetic effects that result from the low temperature structural transition.

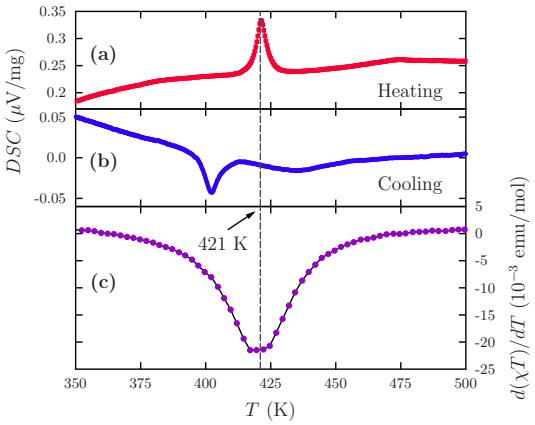

FIG. 1: Peaks within the heating (a) and cooling (b) curves in the DSC measurements indicate an enthalpy of transition ΔH associated with the magnetic phase transition around $T \approx 421$ K. (c) The clear feature in the Fisher heat capacity at $T_N \approx 421$ K verifies the magnetic origin of the transition.

Thermodynamic measurements confirm the presence of the reported magnetic transition around $T_N = 424$ K.[9]

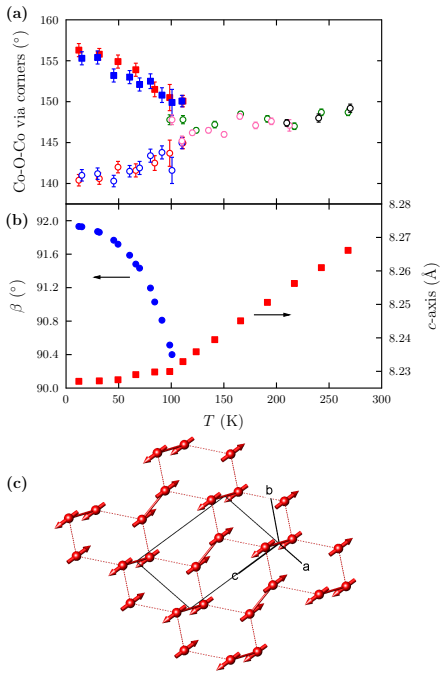

FIG. 2: The behavior of the NPD refined nuclear structure for $CsCoO_2$ associated with the structural phase transition ($T^\star \approx 100$ K): (a) Temperature dependence of the average Co-O2-Co bond angle involving corner-shared oxygen ions, (b) the c-axis lattice constant and the monoclinic angle β within α-$CsCoO_2$. (c) Illustration of the magnetic structure of a single CoO_2 layer within α-$CsCoO_2$.

The results of differential scanning calorimetry (DSC[10]) and the Fisher heat capacity method,[11] are shown in Fig. 1. The DSC thermogram measured on heating displays an endothermic peak centered around 421 K corresponding to the onset of long range AFM ordering, in good agreement with the Néel temperature observed by other methods (see below). The rate of temperature change only slightly affects the enthalpy change but doesn't alter the transition temperature range. There is a substantial change in magnetic entropy and large thermal hysteresis ($\Delta T \approx 15$ K) at T_N between the heating and cooling scans of the DSC plot. In addition, employing the Fisher heat capacity method we have calculated $d(\chi T)/dT$ *vs.* T from our magnetic susceptibility data[9] as shown in Fig. 1(c), displaying a sharp spike consistent with the onset of long range AFM ordering.

In order to elucidate the magnetic structure below T_N and the details of the structural transition around $T^\star$, neutron powder diffraction (NPD) measurements were performed. The NPD patterns collected between 100-$-$700 K are consistent with orthorhombic $Cmca$ symmetry and can be correctly fitted employing the structural model proposed in our earlier work.[9] Below $T^\star \approx 100$ K a displacive structural phase transition from the high temperature $Cmca$ space group (hereafter the β phase) to monoclinic $C2/c$ space group (hereafter the α phase) is observed as the temperature is reduced, producing a set of new reflections and splitting of certain nuclear intensities accompanying the lowering of symmetry. The structural phase transition is apparent in the temperature dependence of the monoclinic angle β, and is accompanied by a peculiarity in the T-dependence of the c-parameter of the unit cell as depicted in Fig. 2(b). While there are no observable features in the temperature dependences of the Co–O average distance, and of the Co–O1–Co bond angles via the edges of the CoO_4 tetrahedra, the Co–O2–Co bond angles via the corners of the CoO_4 tetrahedra also reveal the transition: from two distinct angles in the monoclinic α phase, a single one emerges upon entering the orthorhombic β phase, with a value close to the mean of the two low-T angles [Fig. 2(a)]. This transition is sharp, but results in no discontinuities in the refined values of the bond angles; they approach each other in a gradual manner with increasing temperature. The refinement of the crystal structures above and below $T_N \approx 430$ K (within the paramagnetic and magnetically ordered phases respectively) reveals no significant modification in the nuclear structure, indicating this transition is of solely magnetic origin.

At temperatures below 440 K, in both the α and β phases, the NPD patterns of $CsCoO_2$ also contain magnetic diffraction peaks due to the long range order (LRO) of the magnetic Co^{3+} ion spins. At the structural phase boundary ($T^\star \approx 100$ K), the extra (magnetic) intensities follow the trend of lowering the symmetry, for instance the magnetic intensity contained in the position of the $(1,1,1)$ peak of the crystal structure in the β phase is split into the extra intensity in the $(-1,1,1)$ and $(1,1,1)$ peaks in the patterns of the α phase below $T^\star$, in a similar fashion to the nuclear intensities. However, no magnetic diffraction pattern changes are observed upon cooling below the structural transition, indicating that the magnetic ordering type and pattern is common to both structural phases. (It is possible that this temperature independence of the average Co–O bond distances and of the Co–O–Co bond angles via the edge-sharing O1 oxygen atoms which makes the magnetic ordering so robust against the structural phase transition occurring at $T^\star$.) All the magnetic diffraction peaks have been indexed with the propagation vector $\boldsymbol{k} = (0,0,0)$, for both the α and β phases. The symmetry analysis for this propagation vector and Co ion locations within both the $C2/c$ and $Cmca$ symmetries, has been carried out with the program SARAh-2K,[12] and all symmetry-reasonable magnetic ordering schemes have been verified against the Rietveld refinements. For both the β orthorhombic and the α monoclinic phase, just one irreducible representation is compatible with the magnetic ordering model, satisfactorily explaining the observed magnetic intensity patterns. The magnetic ordering is essentially identical for both the α and β phases and is illustrated in Fig. 2(c) for one buckled CoO_2 layer. This spin order consists of ferromagnetically ordered Co-Co dimers, which are themselves antiferromagnetic ordered. The intradimer Co-Co interatomic distance is significantly shorter than the cor-

responding interdimer Co-Co junctions. In the directions of the closest interdimer distances in the ac-planes (along the diagonal $\boldsymbol{a}+\boldsymbol{c}$ and $\boldsymbol{a}-\boldsymbol{c}$ directions), the ordering between the Co moments in the adjacent dimers is antiferromagnetic, thus leading to the overall compensation of the total magnetization. In the adjacent CoO_2 layer, the magnetic ordering repeats, being naturally offset by a $(0.5, 0.5, 0)$ translation. We find that the direction of the Co^{3+} magnetic moments is along the c-axis of the crystal lattice. The irreducible representations leading to this magnetic ordering type are Γ_1 and Γ_5 for the α monoclinic and β orthorhombic phases of $CsCoO_2$ correspondingly, which in principle do not preclude Co magnetic moment components along the other crystal axes. In the α phase, an admixture of the a-component with identical ordering type as for the actual c-direction could be possible, while for both the α and β phases, an admixture of the ferromagnetic ordering with the b-component could also be symmetrically reasonable. We are unable to assign any significantly meaningful values to the magnitudes of these two ordering types. This means that at all temperatures $T \leq T_N$ where $CsCoO_2$ exhibits magnetic LRO, the only definitely confirmed moment direction is along the c-axis of the unit cell. We have determined unusually low magnitudes for the ordered magnetic moments of 3.089 (2 K) and 2.628 (300 K)μ_B/Co^{3+} for α- and β-$CsCoO_2$, respectively. The suppression of the Co^{3+} magnetic moment can be attributed to strong Co($3d$)O($2p$) hybridization.

To further resolve a microscopic picture of the possible static magnetic structures of $CsCoO_2$, we performed a sequence of density functional theory (DFT) total energy calculations. The density functional plane wave pseudopotential method within the generalized gradient approximation was used as implemented in the CASTEP code.[13,14] A systematic search was performed to categorize the possible AFM structures. In agreement with the NPD results, the lowest energy configuration for both the α and β phases has strongly ferromagnetically aligned Co-Co dimers, with weaker antiferromagnetic order along the Co chains parallel to the crystallographic a-axis [Fig. 3(a)]. The weak AFM interdimer interaction can be easily flipped, as illustrated in Fig. 3(b), at an energy cost of $\Delta E \approx 0.034$ eV/"bond" (for the low-T, α phase). This energy cost may be related to the exchange interaction strength J within the Heisenberg Hamiltonian term for a single exchange bond $\mathcal{H} = -J\boldsymbol{S_1}\cdot\boldsymbol{S_2}$ (employing the single-J convention) via $\Delta E = (1/2)JS_{\uparrow\uparrow}(S_{\uparrow\uparrow}+1)$, where $S_{\uparrow\uparrow} = 2S$ is the spin quantum number of the dimer triplet state. For Co^{3+} ($3d^6$) in the high-spin state, $S = 2$ and therefore $J = \Delta E/10$. Hence the exchange constant for the weak AFM pathway along the corner-shared O^{2-} ion is predicted to be $J' = -39(1)$ K. The ferromagnetic intradimer coupling (via the edge-shared oxygen superexchange pathway) is far stronger. The triplet-singlet energy difference between these Co spins was found to be $\Delta E \approx 0.44$ eV, corresponding to an exchange strength of $J = 511(1)$ K [Fig. 3(c)]. There are a number of possible

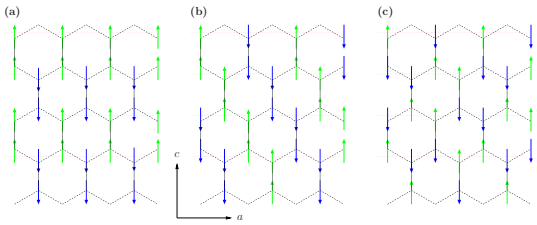

FIG. 3: Schematic diagrams of the spin structure formed by the Co ions are displayed; the Co ions form an extended 2D hexagonal network. The Co ions are positioned at the vertices and interact via edge-sharing oxygen intradimer (solid line) and corner-sharing interdimer (dashed line) superexchange pathways, with Co-Co separations of approximately 2.61 Å and 3.42 Å respectively. (See main text.)

AFM states analogous to Fig. 3(b) (which preserve the FM intradimer spin configuration) that are close in energy and likely to be populated via thermal fluctuations (see below). Ordered moment sizes (constrained to be collinear) were found to be $3.25\mu_B$ per Co ion, with some spin density transferred onto the edge-shared oxygen ions ($1.2\mu_B$ per ion), in good agreement with the low-T value obtained through NPD refinements.

To probe the local magnetism on a timescale distinct from that measured by NPD, muon-spin relaxation (μSR) measurements[15] were made on $CsCoO_2$. For asymmetry spectra obtained in ZF measurements, spontaneous oscillations are clearly visible for temperatures below around 420 K [Fig. 4(a)]. This constitutes unambiguous evidence of quasi-static magnetic LRO throughout the bulk of the material. A clear indication of the transition temperature is given by considering the time-averaged ($t \leq 9.5$ μs) asymmetry data, which drops abruptly upon cooling, where asymmetry is lost as the material enters the magnetically ordered state. Fig. 4(b) shows this drop in average asymmetry, which may be fitted with a Fermi-like step function $\langle A\rangle(T) = A_2 + \frac{A_1 - A_2}{e^{(T-T_c)/w}+1}$, providing a method for extracting the transition temperature[16] by parametrising the continuous step from high- (low-) T asymmetry A_2 (A_1) with mid-point T_c and width w. The fit yielded values of $T_c = 423.7(2)$ K and $w = 1.57(2)$ K, in agreement with the value previously obtained.[9]

Asymmetry specta below T_N were best fitted with the single-frequency oscillatory relaxation function $A(t) = A_1\cos(2\pi\nu t)e^{-\lambda_1 t} + A_2 e^{-\lambda_2 t} + A_b$, where the oscillating amplitude A_1 was fixed to its average value of 5.7%. The non-relaxing baseline contribution A_b is attributable to muons which stop in the Ti sample holder, and, more importantly, to the non-precessing component of muon spins which lie parallel to the local magnetic field. Parameters resulting from this fit are displayed in Fig. 4(c,d). The Larmor precession frequency of the muon ensemble is related to the average magnitude of the static magnetic field B at the muon site via $2\pi\nu = \gamma B$. Here B, and hence ν serves as an effective order parameter for

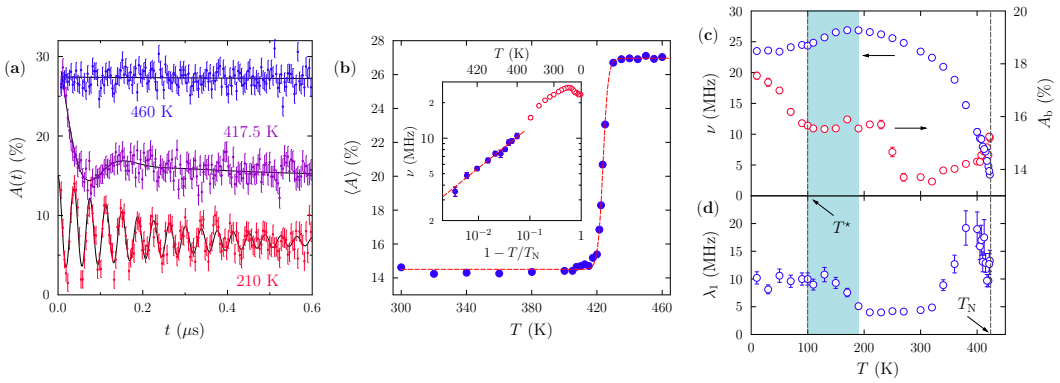

FIG. 4: (a) $A(t)$ spectra, showing the clear single-frequency oscillations in the ordered regime with a fit described in the text (the 210 K data are offset by 10% for clarity). (b) Time-averaged asymmetry near the critical region, displaying an abrupt drop in asymmetry $\Delta A = A_2 - A_1$. The dashed line is the fit described in the text. Inset: scaling plot for the order parameter ν. The linear fit indicates the region where the behaviour is critical. (c) Fitted parameters to the oscillatory relaxation function for all asymmetry data ($t \leq 9.5$ μs) for temperatures $T < T_N$; frequency ν and baseline asymmetry A_b and (d) transverse relaxation rate λ_1. The Néel temperature $T_N = 424$ K and the anomalous temperature region $100 \lesssim T \lesssim 190$ K (including the approximate structural transition temperature $T^\star \approx 100$ K) are indicated.

the LRO.

Upon cooling below T_N, the precession frequency ν increases in the expected manner, and the relaxation rates λ_i peak, as is typical for an AFM phase transition (Fig. 4). Frequencies in the critical region 400 K $\leq T < T_N$ were fitted to $\nu(T) = \nu(0)\,(1 - T/T_N)^\beta$, where $T_N = 424$ K was fixed [see Fig. 4(b) inset]. The fit yielded a value for the critical parameter $\beta = 0.35(2)$,[17] which is consistent with that expected for a 3D Heisenberg antiferromagnet. Moreover, dipole field simulations[10] were performed on $CsCoO_2$ using the proposed magnetic spin structure and crystal parameters obtained from x-ray diffraction at 50 K and 296 K.[9] A Bayesian analysis of this calculation[10,18] shows that the observed muon precession frequencies are fully consistent with a moment size of $2.63\mu_B$ from the neutron measurement and further suggests a muon stopping site approximately 1 Å from the corner-sharing oxygen ions.

In addition to the behavior observed around T_N described above, which is quite typical for an AFM transition, we find that on cooling though the region $T < T_N$, there are a number of additional, notable features in the μSR data. Most noticeably, we find that on cooling below ≈ 190 K the muon precession frequency ν is smoothly suppressed [Fig. 4(c)]. This is accompanied by a steady increase in λ_1, such that λ_1 is larger by a factor of about 2 below $T^\star$ than in the region 200 K $\lesssim T \lesssim$ 300 K [Fig. 4(d)]. Below $T^\star \approx 100$ K, λ_1 and ν both level off at constant values. The decrease of ν below 200 K indicates a reduced value of average magnetic field strength experienced at the muon stopping sites. In the fast fluctuation limit we expect that the relaxation rate $\lambda \propto \langle (B - \langle B \rangle)^2 \rangle \tau$ (i.e. the second moment of the magnetic field distribution multiplied by the correlation time τ[19]) and so the additional dephasing indicates a broadening of the distribution of static magnetic field strengths experienced by the muon ensemble, or an increased correlation time as relaxation channels freeze out on the muon time scale. It is possible that this behaviour reflects the the system exploring some of the energetically similar magnetic states predicted by the DFT calculations described above. These states are realized by flipping the overall spin of a dimer, while preserving their FM intradimer spin configuration [Fig. 3(b)]. Although this could conceivably lead the muon ensemble to experience a broader static magnetic field distribution, with a lower mean field strength, one would expect this to occur below $T^\star$ rather than above it. Moreover, the refined cobalt moment sizes from NPD data (shown in the SI[10]) do not show this suppression below 200 K, suggesting that the effect could be dynamic and related to the issue of timescale. Such effects are therefore not seen in the neutron measurements as these effectively take a 'snapshot' of the spin distribution, when compared to the muon GHz timescale.

Additional evidence for the influence of dynamics comes from the baseline asymmetry A_b, which increases abruptly at around 250 K and upon further cooling below $T^\star$ gradually increases further [Fig. 4(c)]. Since relaxation of those muon spins that initially point along the direction of the local magnetic field can only be achieved by dynamic relaxation precesses, the increase of such a non-relaxing signal is usually indicative of a freezing of relaxation processes. We therefore have evidence for an initial, abrupt freezing of some relaxation channels around 250 K, prefiguring the suppression of the precession frequency ν, followed by a further, smooth increase that seems to be reminiscent of the size of the monoclinic distortion as indicated by both the change in unit cell angle β and the splitting of the corner-shared bond angle Co–O2–Co (Fig. 2). This monoclinic distortion leads to a disproportionation of the corner-sharing

oxygen bond angles; above $T^\star$ there is one unique value of about 150°, whereas below there appear two classes of bond with angles of around 140° and 155°.[10] These values lie within the linear GKA rule regime, but not particularly close to the fully linear angle of 180° (which leads to strong AFM coupling), hence the weaker AFM exchange interaction strength J'. Meanwhile the edge-sharing intradimer bond angle only slightly deviates from 90° both above and below $T^\star$ (88° and 86° respectively[10]) and therefore displays a strong FM superexchange interaction as expected from GKA. The weaker AFM interdimer coupling drives the transition to LRO, and so the system would be sensitive to the bifurcation of the corner-sharing oxygen bond angle below $T^\star$, where the AFM exchange interaction strength J' would also split into two unequal values. When these superexchange pathways become inequivalent in the monoclinic phase it is possible that this allows some relaxation channels to freeze out, leading to a greater static component of the magnetic field, and hence the increase in non-relaxing asymmetry A_b observed.

In conclusion, neutron powder diffraction has enabled the determination of the microscopic magnetic structure of $CsCoO_2$ below the Néel temperature. The tetrahedrally coordinated high-spin ($S = 2$) Co^{3+} ions form a spin configuration comprising strongly FM linked dimers, with weaker AFM interdimer superexchange interactions creating the extended LRO within the extended CoO_2 planes. This spin configuration is observed both above and below a structural phase transition around $T^\star \approx 100$ K, and is supported by DFT calculations. The bifurcation of bond angles, and hence superexchange pathway interaction strengths pertaining to the weaker AFM interdimer interactions, result in a complicated freezing of relaxation processes on the muon timescale.

This work is partly based on the results of experiments carried out at the Swiss spallation neutron source SINQ and Swiss muon source SμS, Paul Scherrer Institut, Villigen, Switzerland. We are grateful for the provision of beamtime, and to Alex Amato for muon experimental assistance. We also wish to thank UKCP and the Archer HPC facility for computer time. This work is supported by the EPSRC (UK).

[1] A. Maignan , C. Michel, A. C. Masset, C. Martin, and B. Raveau, Eur. Phys. J. B **15**, 657 (2000).
[2] J. B. Goodenough, Progress in Solid State Chemistry, edited by H. Reiss (Pergamon, Oxford, 1965), Vol. 5, p. 145.
[3] M. Pouchard, A. Villesuzanne, J.-P. Doumerc, J. Solid State Chem. **162**, 282 (2001).
[4] M. Jansen and R. Hoppe, Z. Anorg. Allg. Chem. **417**, 31 (1975).
[5] C. Delmas, C. Fouassier, and P. Hagenmuller, J. Solid State Chem. **13**, 165 (1975).
[6] M. Sofin, E. M. Peters, and M. Jansen, J. Solid State Chem. **177**, 2550 (2004).
[7] J. Birx and R. Hoppe, Z. Anorg. Allg. Chem. **597**, 19 (1991).
[8] N. Stüßer, M. Sofin, R. Bircher, Hans-Ulrich Gdel, and M. Jansen Chem. Eur. J. **12**, 5452 (2006).
[9] N. Z. Ali, J. Nuss, R. K. Kremer, and M. Jansen, Inorg. Chem. **51**, 12336 (2012).
[10] The Supplemental Information contains further experimental details of synthesis, DSC, NPD and μSR measurements. Full structural details obtained from Rietveld refinements of NPD data are also provided.
[11] M. E. Fisher, Philos. Mag. **7**, 1731 (1962).
[12] A. S. Wills, Physica B. **276**, 680 (2000), program available from [www.ccp14.ac.uk].
[13] S. J. Clark, M. D. Segall, C. J. Pickard, P. J. Hasnip, M. I. J. Probert, K. Refson and M. C. Payne, Z. Kristallogr. **220**, 567 (2005).
[14] P. J. Hasnip, K. Refson, M. I. J. Probert, J. R. Yates, S. J. Clark and C. J. Pickard, Phil. Trans. R. Soc. A **372**, 20130270 (2014).
[15] S. J. Blundell, Contemp. Phys. **40**, 175 (1999).
[16] A. J. Steele, T. Lancaster, S. J. Blundell, P. J. Baker, C. Baines, M. M. Conner, H. I. Southerland, J. L. Manson and J. A. Schleuter, Phys. Rev. B **84**, 064412 (2011).
[17] The value of the critical parameter β for a given fitted frequency ν was found to be sensitive to the time range over which the asymmetry spectra were fitted. The quoted value of 0.35 was obtained for fits over early times only ($t \leq 1$ μs), which are most sensitive to the behavior of the oscillations.
[18] S. J. Blundell, A. J. Steele, T. Lancaster, J. D. Wright and F. L. Pratt, Physics Procedia **30**, 113 (2012).
[19] R. S. Hayano, Y. J. Uemura, J. Imazato, N. Nishida, T. Yamazaki and R. Kubo, Phys. Rev. B **20**, 850 (1979).